The 9th European Congress on Computational Methods in Applied Sciences and Engineering
ECCOMAS Congress 2024
3–7 June 2024, Lisboa, Portugal

NUMERICAL METHODS AND RELAXATION TECHNIQUES FOR DIFFUSE INTERFACE MODELS IN HIGH-VELOCITY TWO-PHASE FLOW SIMULATIONS

WARD HAEGEMAN[1,2], JOËL DUPAYS[1], CLÉMENT LE TOUZE[1] and MARC MASSOT[2]

[1] Department of Multi-Physics for Energetics, ONERA
Université Paris-Saclay, F-91123 Palaiseau - France

[2] Centre de Mathématiques Appliquées, CNRS École polytechnique
Institut Polytechnique de Paris, 91120 Palaiseau - France

email: ward.haegeman@polytechnique.edu

Key words: two-phase flows, multi-fluid models, relaxation processes, high-speed flows

Summary. Several strategies to solve the 5-equation model of Kapila relying on instantaneous pressure relaxations have been proposed in the literature. These methods rely on the introduction of an interfacial pressure which does not exist in the 5-equation model. In this paper, a detailed analysis of the pressure relaxation process is provided with emphasis on the role of interfacial pressure and on how the process differs from the pressure-temperature relaxation process. Accurate relaxation methods are developed and the impact of the interfacial pressure on the numerical robustness but also on the convergence of the method towards weak solutions is investigated. It is shown to be a key parameter of the pressure relaxation process while playing no role in the instantaneous pressure-temperature relaxation. A set of challenging numerical test cases are presented and used to compare the different relaxation processes.

1 INTRODUCTION

Two-phase flows appear in many industrial applications or natural phenomena, and their understanding relies on accurate numerical simulations. In the context of separated interface flows, several modelling strategies have been proposed; we focus on the class of two-fluid models. Among these models, the one proposed by Baer and Nunziato [1] in the context of deflagration-to-detonation transition in granular explosives has been extended to liquid-gas flows by Saurel and Abgrall [2]. It allows the two phases to be fully out-of-equilibrium as each phase has its own pressure, temperature and velocity. Assuming some of these quantities remain at equilibrium during the flow allows one to derive a hierarchy of reduced order models ranging from the original 7-equation model to a 4-equation model [3, 4, 5]. The 5-equation model derived by Kapila [3] belongs to this hierarchy. Many numerical schemes have been developed for this model [6, 7, 8, 9] with several relying on the instantaneous pressure relaxation approach [7, 8, 10]. A similar strategy relying on an instantaneous pressure-temperature relaxation allows the numerical simulation of the 4-equation model. However, the mathematical structure of both models differs: while the 4-equation model is conservative, the 5-equation model involves a non-conservative product and does not posses a complete set of jump conditions. Moreover, convergence to weak solutions is only established for the pressure-temperature relaxation scheme and the pressure relaxation approach suffers from theoretical difficulties which are still under investigation. In this paper, we propose a detailed analysis and comparison of the instantaneous relaxation processes. We provide theoretical insights concerning pressure relaxation parameters as well as accurate methods, which are then used to investigate the effect of these parameters

on several challenging numerical test cases. The choice of these parameters is shown to be paramount to ensure the robustness of the scheme. The pressure relaxation scheme is then compared to the pressure-temperature relaxation scheme on a shock-droplet interaction case. The outline of this paper is the following. In Section 2, we present the 5-equation model and recall some of its properties, in Section 3, the numerical strategy relying on an instantaneous relaxations of the 6-equation model is presented, while the instantaneous relaxation processes itself are described in detail and analysed in Section 4 with emphasis given on the difference between pressure relaxation and pressure-temperature relaxation. Numerical results comparing the relaxation processes and illustrating the impact of pressure relaxation parameters are given in Section 5.

2 PRESENTATION OF THE MODEL

We consider is the five-equation model of Kapila [3]. It is derived through a Chapman-Enskog-like expansion of the 7-equation model of Baer and Nunziato [1] in the limit of instantaneous relaxation towards equilibrium of the pressures and velocities. The model writes as follows:

$$\frac{\partial}{\partial t}\alpha_1 + \boldsymbol{u}\cdot\nabla\alpha_1 + \alpha_1\alpha_2\frac{\rho_1 c_1^2 - \rho_2 c_2^2}{\alpha_2\rho_1 c_1^2 + \alpha_1\rho_2 c_2^2}\nabla\cdot\boldsymbol{u} = 0, \tag{1a}$$

$$\frac{\partial}{\partial t}(\alpha_1\rho_1) + \nabla\cdot(\alpha_1\rho_1\boldsymbol{u}) = 0, \tag{1b}$$

$$\frac{\partial}{\partial t}(\alpha_2\rho_2) + \nabla\cdot(\alpha_2\rho_2\boldsymbol{u}) = 0, \tag{1c}$$

$$\frac{\partial}{\partial t}(\rho\boldsymbol{u}) + \nabla\cdot(\rho\boldsymbol{u}\otimes\boldsymbol{u}) + \nabla p = \boldsymbol{0}, \tag{1d}$$

$$\frac{\partial}{\partial t}(\rho E) + \nabla\cdot((\rho E + p)\boldsymbol{u}) = 0. \tag{1e}$$

We use the following notations for $k = 1, 2$, α_k is the volume fraction of phase k, the volume fractions sum up to unity. The phasic densities are denoted ρ_k, the mixture density, $\rho = \alpha_1\rho_1 + \alpha_2\rho_2$ and the phasic sound velocity, c_k. The mixture velocity is denoted $\boldsymbol{u}$ and $E = e + \frac{1}{2}|\boldsymbol{u}|^2$ represents the specific total energy with e the specific internal energy of the mixture. The two phases are in pressure equilibrium at all times and their common pressure p is found by solving

$$\text{Find } p \text{ such that } Y_1 e_1^{\mathrm{EOS}}(\rho_1, p) + Y_2 e_2^{\mathrm{EOS}}(\rho_2, p) = E - \tfrac{1}{2}|\boldsymbol{u}|^2, \tag{2}$$

here we have introduced the notation $Y_k = \alpha_k\rho_k/\rho$ for the mass fraction of phase k as well as the energy equations of state. Although the model assumes pressure equilibrium, it does not assume the phases to be in thermal equilibrium, as each phase has its own temperature:

$$T_k = T_k^{\mathrm{EOS}}(\rho_k, p). \tag{3}$$

For the numerical results of Section 5, we will use a stiffened gas equation of state for each phase such that

$$p_k = (\gamma_k - 1)\rho_k e_k - \gamma_k p_{\infty,k}, \quad T_k = \frac{p_k + p_{\infty,k}}{(\gamma_k - 1)\rho_k c_{v,k}}, \tag{4}$$

where $\gamma_k > 1$, $p_{\infty,k}$ and $c_{v,k} > 0$ are the EOS parameters of the k^{th} phase.
The model is unconditionally hyperbolic. In one dimension, its Jacobian matrix has 5 real eigenvalues $\lambda = u - c_{\mathrm{w}}$, $\lambda = u$ and $\lambda = u + c_{\mathrm{w}}$ where c_{w} is the mixture sound velocity, also called Wood's sound velocity [11] and is defined through

$$\frac{1}{\rho c_{\mathrm{w}}^2} = \frac{\alpha_1}{\rho_1 c_1^2} + \frac{\alpha_2}{\rho_2 c_2^2}. \tag{5}$$

The material wave $\lambda = u$ has multiplicity 3 and is associated to a linearly degenerate characteristic field while the acoustic waves $\lambda = u \pm c_{\mathrm{w}}$ are simple and genuinely non-linear.
The model also admits a supplementary conservation law for the mixture entropy

$$\frac{\partial}{\partial t}(\rho s) + \nabla \cdot (\rho s \boldsymbol{u}) = 0, \qquad \rho s = \alpha_1 \rho_1 s_1 + \alpha_2 \rho_2 s_2. \tag{6}$$

However, the non-conservative nature of the volume fraction equation (1a) does not allow for shock relations to be uniquely defined. Although there are some systems for which non-conservative products can be uniquely defined and appropriate numerical schemes constructed [12, 13], it is however not the case for the model under consideration. This leads to both theoretical and numerical difficulties when dealing with weak solutions [14, 15, 16, 17]. One way to define jump conditions for a non-conservative system is through travelling wave solutions: a parabolic diffusion term is added to the equation resulting in a smooth travelling wave profile connecting a left state to a right state. In the limit of a vanishing diffusion a shock profile is obtained. For conservative systems, the resulting shock profile satisfies the well-known Rankine-Hugoniot conditions; for non-conservative systems however, the resulting shock profile depends on the diffusion matrix. A consequence of this fact is that different numerical schemes can converge towards different numerical solutions as each scheme has its own numerical diffusion matrix [17, 18]. Therefore, the key issues for such models is to identify the parameters of the numerical scheme which can affect the structure of the numerical diffusion and to evaluate the impact these parameters have on weak solutions.

3 NUMERICAL STRATEGY

The numerical strategy that we follow originates from the works of Saurel et al. [7] and is inspired from the theory of relaxation schemes [19, 20, 21]. We consider a 6-equation, 2-pressure model endowed with stiff pressure relaxation terms. A Chapman-Enskog expansion shows that in the limit of infinitely fast pressure relaxation, we recover the 5-equation model [3]. The numerical scheme we consider consists in a two-step procedure. Time stepping is done by first solving the 6-equation model without any relaxation source terms — which will be referred to as homogeneous 6-equation model in the following — and then, relaxing the solution until pressure equilibrium is reached (*ie* instantaneous relaxation, see Section 4). The original approach considers a 6-equation model with equations for the internal energies, an energy correction procedure is then necessary to ensure the conservation of the total energy [7, 9]. However, we have observed that these corrections can compromise the robustness of the numerical scheme as they do not guarantee the positivity of the temperatures, therefore it is preferable to use total energy equations following [8]. The 6-equation model that we consider writes as follows,

$$\frac{\partial}{\partial t}\alpha_1 + \boldsymbol{u} \cdot \nabla \alpha_1 = \frac{p_1 - p_2}{\varepsilon}, \tag{7a}$$

$$\frac{\partial}{\partial t}(\alpha_1 \rho_1) + \nabla \cdot (\alpha_1 \rho_1 \boldsymbol{u}) = 0, \tag{7b}$$

$$\frac{\partial}{\partial t}(\alpha_2 \rho_2) + \nabla \cdot (\alpha_2 \rho_2 \boldsymbol{u}) = 0, \tag{7c}$$

$$\frac{\partial}{\partial t}(\rho \boldsymbol{u}) + \nabla \cdot (\rho \boldsymbol{u} \otimes \boldsymbol{u}) + \nabla \overline{p} = \boldsymbol{0}, \tag{7d}$$

$$\frac{\partial}{\partial t}(\alpha_1 \rho_1 E_1) + \nabla \cdot (\alpha_1 (\rho_1 E_1 + p_1)\boldsymbol{u}) - \boldsymbol{u} \cdot (Y_2 \nabla(\alpha_1 p_1) - Y_1 \nabla(\alpha_2 p_2)) = -p_I \frac{p_1 - p_2}{\varepsilon}, \tag{7e}$$

$$\frac{\partial}{\partial t}(\alpha_2 \rho_2 E_2) + \nabla \cdot (\alpha_2 (\rho_2 E_2 + p_2)\boldsymbol{u}) + \boldsymbol{u} \cdot (Y_2 \nabla(\alpha_1 p_1) - Y_1 \nabla(\alpha_2 p_2)) = +p_I \frac{p_1 - p_2}{\varepsilon}, \tag{7f}$$

and the homogeneous 6-equation model is obtained by discarding the right-hand side source terms. The notations previously introduced are still valid. New notations correspond to the phasic total energy $E_k = \frac{1}{2}|\boldsymbol{u}|^2 + e_k$ (with e_k the phasic internal energy), phasic pressure p_k, the mixture pressure $\overline{p} = \alpha_1 p_1 + \alpha_2 p_2$ and the interfacial pressure p_I which will be discussed later on. As the pressure equilibrium assumption has been lifted in this model, each phase has its own Gibbs relation and we have

$$p_k = p_k^{\mathrm{EOS}}(\rho_k, e_k), \qquad T_k = T_k^{\mathrm{EOS}}(\rho_k, e_k). \tag{8}$$

The model is unconditionally hyperbolic. In one dimension its Jacobian matrix admits 6 real eigenvalues $\lambda = u - c_\mathrm{f}$, $\lambda = u$ and $\lambda = u + c_\mathrm{f}$ where c_f is the mixture sound velocity, sometimes referred to as frozen sound speed, and is given by

$$\rho c_\mathrm{f}^2 = \alpha_1 \rho_1 c_1^2 + \alpha_2 \rho_2 c_2^2. \tag{9}$$

The material wave $\lambda = u$ has multiplicity 4 and is associated to a linearly degenerate characteristic field while the acoustic waves $\lambda = u \pm c_\mathrm{f}$ are simple and genuinely non-linear. Since the material wave is linearly degenerate, the volume fraction equation (7a) now has a non-conservative product which is well defined, the phasic energy equations (7e,7f) however have non-conservative products which are not uniquely defined.

The time discretization strategy is as follows. We denote by $\mathscr{H}_{\Delta t}$ the time step operator of the homogeneous part of (7), and $\mathscr{R}$ the instantaneous pressure relaxation operator. The vector of unknown $\boldsymbol{q}$ is then updated in time according to the following formula

$$\boldsymbol{q}^{n+1} = \mathscr{R}\mathscr{H}_{\Delta t}\boldsymbol{q}^n, \tag{10}$$

which is reminiscent of the Lie-Trotter splitting but is in fact a projection scheme. Indeed, in the limit $\varepsilon \to 0$, the relaxation operator does not depend on the time-step and becomes a local non-linear projection on the pressure equilibrium manifold. Formula (10) results in a first-order in time scheme for the 5-equation model (1). Higher order accuracy can be achieved using a SSP Runge-Kutta method [22] with relaxations for each stage [23]. Space discretization is achieved through a finite-volume method, a HLLC Riemann solver is used, approximate jump conditions are provided to close the intermediate states and the non-conservative term is treated similarly as in [7, 24].

When the pressure relaxation operator $\mathscr{R}$ is replaced by an instantaneous pressure and temperature relaxation operator, formula (10) yields a first-order in time scheme for the 4-equation model [25]. The 4-equation model, similar to the two-species Euler equations, is fully conservative and obtained by discarding the volume fraction equation (1a) from system (1) and assuming pressure and temperature equilibrium for its thermodynamic closure. The mathematical properties of the 5-equation model and the 4-equation concerning weak solutions are very different as only the 4-equation model has a complete set of jump conditions; this can be linked to a difference in the structure of the corresponding relaxation operators. The following section is dedicated to the instantaneous relaxation processes with emphasis on the difference between the pressure relaxation and the pressure-temperature relaxation.

4 INSTANTANEOUS RELAXATION PROCESSES

4.1 Some theoretical insights about the role of the interfacial pressure

We now discuss the pressure relaxation source term corresponding to the right-hand side of (7). The source term on the volume fraction equations drives the system towards pressure

equilibrium. However, the volume fraction source term alone is not compatible with the entropy inequality. The energy equations' source terms restore the thermodynamic compatibility of the relaxation process; they account for the energy exchanges between the phases resulting from the volume changes that take place during this process. These exchanges are driven by an interfacial pressure p_I. This pressure is non-existing in the 5-equation model, and should therefore be considered to be a numerical parameter of the relaxation scheme, it is usually chosen such that $\min(p_1, p_2) \leq p_I \leq \max(p_1, p_2)$.

Several choices for the interfacial pressure have been used in the literature, we will now clarify the impact of this choice in the limit of an instantaneous pressure relaxation. In the following, for a given quantity $\mathcal{X}$, we will denote $\mathcal{X}^{(0)}$ and $\mathcal{X}^\star$ the value of $\mathcal{X}$ before and after the relaxation process respectively. Since several quantities remain unchanged by the relaxation process, the number of equations can be reduced to two. They write

$$\frac{\mathrm{d}\alpha_1}{\mathrm{d}t} = \frac{p_1 - p_2}{\varepsilon}, \tag{11a}$$

$$\frac{\mathrm{d}e_1}{\mathrm{d}t} = -\frac{p_I}{(\alpha_1\rho_1)^{(0)}}\frac{p_1 - p_2}{\varepsilon}. \tag{11b}$$

Knowing α_1 and e_1 we have $\alpha_2 = 1 - \alpha_1$, $\rho_k = (\alpha_k\rho_k)^{(0)}/\alpha_k$ and $e_2 = (e - Y_1^{(0)}e_1)/Y_2^{(0)}$ thus the thermodynamic state of each phase is determined. The velocity field is unaffected by the pressure relaxation process.

In the limit of instantaneous relaxation ($\varepsilon \to 0$), eq. (11a) gives $p_1 = p_2$, however the system is not endowed with a sufficient amount of constraints for this equation to fully determine the relaxed state. Instead, it defines a one-dimensional manifold of equilibrium states which has an implicit parametrization $\alpha^\star \mapsto e_1^\star$ defined by

$$p_1^{\mathrm{EOS}}\left(\tfrac{(\alpha_1\rho_1)^{(0)}}{\alpha_1^\star},\, e_1^\star\right) - p_2^{\mathrm{EOS}}\left(\tfrac{(\alpha_2\rho_2)^{(0)}}{1-\alpha_1^\star},\, \tfrac{e^{(0)} - Y_1^{(0)}e_1^\star}{Y_2^{(0)}}\right) = 0. \tag{12}$$

The correct relaxed state is then found by considering eq. (11b), in the limit $\varepsilon \to 0$ it becomes

$$\frac{\mathrm{d}e_1}{\mathrm{d}\alpha_1} = -\frac{p_I}{(\alpha_1\rho_1)^{(0)}}, \tag{13}$$

which defines a thermodynamic path starting from $(\alpha_1^{(0)},\, e_1^{(0)})$ and entirely determined by the interfacial pressure. The final state $(\alpha_1^\star,\, e_1^\star)$ is then obtained as the intersection of the equilibrium manifold (12) and the thermodynamic path (13). One of the consequences of this dependence of the equilibrium state with respect to the choice of interfacial pressure, is that a change of interfacial pressure may modify the numerical diffusion [1]. In turn, this may lead to a modification in the numerical volume fraction jump condition that is obtained with the scheme (recall that there is no clear mathematical definition for the volume fraction jump condition for the 5-equation model).

If the numerical scheme is employed with time-step Δt, it may seem reasonable to consider that in smooth regions $p_1^{(0)} - p_2^{(0)} = \mathcal{O}(\Delta t)$ since at the start of the hyperbolic step, the state is at pressure equilibrium. One would then expect that the choice of interfacial pressure plays little to no role. However, for liquid-gas flows, the pressure law of the liquid is extremely stiff when compared to the pressure law of the gas and substantial pressure differences can still occur. This fact will be illustrated in Section 5.1.

[1] See for instance [21] for a link between Chapman-Enskog expansion and numerical diffusion of the time discretization – note however that our scheme does not fit within the framework presented in this reference

We now discuss the pressure-temperature relaxation process through which we obtain a numerical scheme for the 4-equation model instead of the 5-equation model. When instantaneous temperature relaxation is added, the equilibrium state does not depend on the choice of interfacial pressure. This is because we get the additional constraint

$$T_1^{\mathrm{EOS}}\left(\tfrac{(\alpha_1\rho_1)^{(0)}}{\alpha_1^\star},\, e_1^\star\right) - T_2^{\mathrm{EOS}}\left(\tfrac{(\alpha_2\rho_2)^{(0)}}{1-\alpha_1^\star},\, \tfrac{e^{(0)}-Y_1^{(0)}e_1^\star}{Y_2^{(0)}}\right) = 0, \tag{14}$$

which, together with eq. (12), fully determines the equilibrium state. The physical interpretation is that interfacial pressure determines the energy exchanges due to the work of volume changes, but now heat exchanges redistribute the energy in the system. Therefore in the case of pressure-temperature relaxation, different interfacial pressures lead to different thermodynamic paths but the equilibrium state is the same whereas for pressure relaxation only, the equilibrium state depends on the thermodynamic path. This is coherent with the fact that the 4-equation model is conservative and the Rankine-Hugoniot jump conditions hold. Moreover the convergence for weak solutions of the relaxation scheme can be established following the framework presented in [20, 21], this is however not the case for the pressure relaxation scheme.

4.2 Relaxation techniques

Most methods for the instantaneous pressure relaxation process proposed in the literature rely on an approximate computation of the equilibrium state [7, 26]. For these methods there is no guarantee of entropy consistency, and in extreme cases some of them can violate the thermodynamic constraints and lead to negative temperatures. Moreover, these methods rely on the assumption that the initial state is close to equilibrium, however in practice large initial pressure differences can occur — mainly because of the stiffness of the equation of state of the liquid — leading to numerical errors which can affect the physical solutions obtained.

In order to properly study the impact of the choice of interfacial pressure on the numerical scheme we require an accurate and robust resolution of the relaxation process which preserves all thermodynamic constraints. Our strategy consists in identifying interfacial pressures which allow for an exact parametrization of the thermodynamic path (13). Writing the phasic entropy equations, we get

$$\alpha_k\rho_k T_k \frac{\mathrm{D}s_k}{\mathrm{D}t} = (-1)^k(p_I - p_k)\frac{p_1 - p_2}{\varepsilon}. \tag{15}$$

Therefore if the interfacial pressure is taken as the pressure of one of the phases, $p_I = p_k$ for either $k = 1$ or $k = 2$, we get that the thermodynamic path coincides with the isentrope of phase k and all the entropy production is concentrated in the other phase. This additional constraint allows for a direct computation of the corresponding equilibrium state as it allows to reduce eq. (12) to an equation with a single unknown.

Another choice for the interfacial pressure that is of particular interest is the mixture pressure $p_I = \overline{p}$. In the case where both equations of state are stiffened gas laws (4), this choice results in an analytical expression of the thermodynamic path. Indeed, ODE (13) then writes

$$\frac{\mathrm{d}e_1}{\mathrm{d}\alpha_1} = A + B\alpha_1 + Ce_1 \quad \text{with} \quad A = \tfrac{\gamma_2 p_{\infty,2} - (\gamma_2-1)(\rho e)^{(0)}}{(\alpha_1\rho_1)^{(0)}}, \quad B = \tfrac{\gamma_1 p_{\infty,1} - \gamma_2 p_{\infty,2}}{(\alpha_1\rho_1)^{(0)}}, \quad C = \gamma_2 - \gamma_1, \tag{16}$$

and has analytical solution

$$e_1 = e_1(\alpha_1) = -\frac{B+AC}{C^2} - \frac{B}{C}\alpha_1 + \left(e_1^{(0)} + \frac{B}{C}\alpha_1^{(0)} + \frac{B+AC}{C^2}\right)\exp\left[C\left(\alpha_1 - \alpha_1^{(0)}\right)\right]. \tag{17}$$

Similarly as before, using this expression together with eq. (12) leads to a closed equation for $\alpha_1^\star$ which can be solved using a Newton method.

Using the analytical expressions of the thermodynamic paths ensures entropy consistency, preservation of all thermodynamic constraints and allows for very accurate computations of the

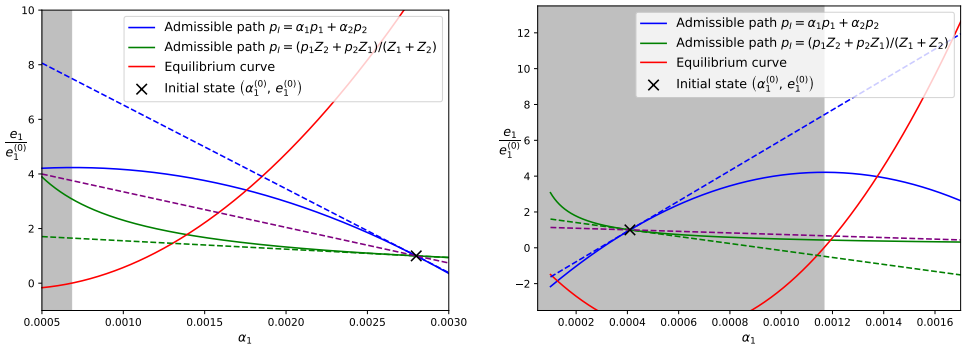

(a) (b)

Figure 1: Two pressure relaxation processes in the (α_1, e_1) plane for two different interfacial pressures, exact (full lines) and linearised (dotted lines) paths.

equilibrium state. Moreover, the proposed relaxation procedure induces almost no additional cost as the method converges rapidly and since the relaxation is a local process, it can easily be parallelized. We end this section by illustrating two relaxation processes which are shown in the (α_1, e_1) plane in Figure 1, the interfacial pressure considered are

$$p_I = \overline{p} = \alpha_1 p_1 + \alpha_2 p_2, \qquad p_I = \frac{Z_2 p_1 + Z_1 p_2}{Z_1 + Z_2} \text{ with } Z_k = \rho_k c_k. \tag{18}$$

For the first case, we used the analytical expression (17); for the second, we considered an expression which is often proposed in the literature and used an embedded Runge-Kutta method to solve ODE (13). The thermodynamic paths, plotted for these two different cases (full blue and green lines), intersect the equilibrium curve (red line) at the equilibrium state. Dotted lines correspond to approximate methods which linearise the thermodynamic path [7, 8]. The purple curve is the method used in [7, 10], it relies on an implicit linearisation of the thermodynamic path making it independent of the choice of interfacial pressure. The shaded area corresponds to volume fractions for which the equilibrium state (vertical projection on the equilibrium curve) is not admissible (negative temperature for one of the phases). The exact thermodynamic paths always intersect the equilibrium curve in the admissible region thus ensuring positivity of the equilibrium state; among the approximate methods described previously, only the implicit approximate method has this property. In Figure 1b, the initial state is located in the shaded area and gives an example of positivity loss for one of the approximate methods (see the dotted green line). This case also shows the strong dependence of the relaxed state on the choice of interfacial pressure in the instantaneous pressure relaxation process.

For the pressure-temperature relaxation process, eqs. (12) and (14) form a closed system and the equilibrium state can be computed directly with a root finding algorithm such as the Newton-Raphson method. Moreover in the case where both equations of state are stiffened gas laws analytical expression can be derived as the equilibrium pressure can be expressed as a root of a quadratic equation [8].

5 NUMERICAL RESULTS

We now present a set of three numerical test-cases which have been chosen to illustrate the impact of the relaxation process on different aspects of the numerical scheme, namely its robustness (double rarefaction case, Sec. 5.1), the convergence towards weak solutions (extreme epoxy-spinel shock, Sec. 5.2) and the ability of the proposed strategy to capture properly the physics of high-speed flows (early stages of a shock-droplet interaction case, Sec. 5.3).

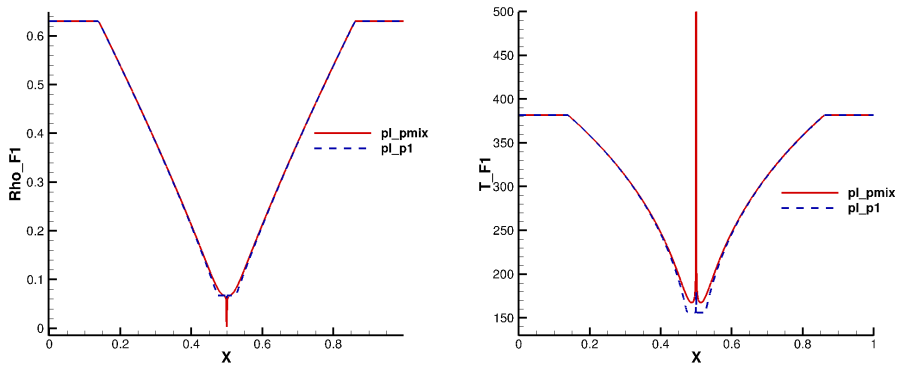

Figure 2: Gas density (left) and temperature (right) for the double rarefaction Riemann problem.

5.1 Double rarefaction in a liquid dominated mixture

We consider the double rarefaction Riemann problem in quasi-pure liquid proposed in [27]. The gas has phase index 1; the stiffened gas EOS parameters used are $\gamma_1 = 1.4$, $p_{\infty,1} = 0\,\mathrm{GPa}$, $c_{v,1} = 1040\,\mathrm{J\,kg^{-1}\,K^{-1}}$ and $\gamma_2 = 4.4$, $p_{\infty,2} = 6 \times 10^8\,\mathrm{GPa}$, $c_{v,2} = 1816\,\mathrm{J\,kg^{-1}\,K^{-1}}$. The initial condition is made up by two states with identical thermodynamic conditions $\rho_1 = 0.63\,\mathrm{kg\,m^{-3}}$, $\rho_2 = 1150\,\mathrm{kg\,m^{-3}}$ and $\alpha_1 = 1 \times 10^{-2}$ and $p = 1 \times 10^5\,\mathrm{Pa}$, and with opposing velocities $u^{\mathrm{L}} = -2\,\mathrm{m\,s^{-1}}$, $u^{\mathrm{R}} = 2\,\mathrm{m\,s^{-1}}$; the states are separated at $x = 0.5\,\mathrm{m}$. Computations are done using the first order method on a fine mesh (4000 cells) at CFL 0.4, the final time is $t_f = 3.2\,\mathrm{ms}$. Interfacial pressures considered here are the mixture pressure $p_I = \overline{p}$ and the gas pressure $p_I = p_1$. Because the liquid volume fraction is close to one, the results with $p_I = p_2$ are almost identical to those shown for the mixture pressure. The results for gas density and gas temperature are shown in Figure 2. We observe a clear difference in the robustness of the computation depending on the interfacial pressure. This is because the solutions to this problem for the 5-equation model and the 6-equation model are very different. In the 6-equation model, each phase follows its own thermodynamics and since we use a stiffened gas equation of state, negative pressures down to $-p_{\infty,2}$ are allowed. In the initial stages of the computation, the hyperbolic step of the scheme tries to generate a middle state for the Riemann problem with a negative liquid pressure. This is not allowed for the 5-equation model, which considers only a mixture pressure that must be valid for both phases. This constraint is enforced during the relaxation process. This issue can result in a negative interfacial pressure depending on its chosen expression. As the energy exchanges during the relaxation process are driven by the interfacial pressure (see (13)) when its sign changes, so does the sign of the energy exchanges. In Fig. 2 this phenomenon is observed for the case $p_I = \overline{p}$: negative interfacial pressures cause the energy exchanges to revert direction during the relaxation process and the gas undergoes a heating expansion causing a temperature instability. For the case $p_I = p_1$, positivity of the interfacial pressure is always guaranteed and the gas cools down when it expands during the relaxation process; as a result, only a small temperature peak can be observed. This illustrates how the interfacial pressure parameter can have a major impact on the robustness of the scheme.

5.2 Extreme shock in an epoxy-spinel mixture

We now consider the Riemann problem proposed in [7] corresponding to an extreme shock propagating in an epoxy-spinel mixture. Epoxy has phase index 1; the stiffened gas EOS parameters used are $\gamma_1 = 2.43$, $p_{\infty,1} = 5.3\,\mathrm{GPa}$ and $\gamma_2 = 1.62$, $p_{\infty,2} = 141\,\mathrm{GPa}$. The initial condition is made up by two states at rest with $\rho_1 = 1185\,\mathrm{kg\,m^{-3}}$, $\rho_2 = 3622\,\mathrm{kg\,m^{-3}}$ and $\alpha_1 = 0.5954$, the pressure is $p^{\mathrm{L}} = 2 \times 10^{11}\,\mathrm{Pa}$ in the left state and $p^{\mathrm{R}} = 1 \times 10^5\,\mathrm{Pa}$ in the right state; the states

are separated at $x = 0.6\,\mathrm{m}$. The problem is solved using the first-order scheme on two different meshes (4000 and 8000 cells) at a CFL number of 0.4, the final time is $t_f = 3.5 \times 10^{-5}\,\mathrm{s}$. Results for the epoxy volume fraction for different choices of interfacial pressure are shown on Figure 3.

The results show that mesh convergence has been attained and that for each case a different intermediate state for the Riemann problem is obtained. Here we have used the two extreme cases $p_I = p_1$ and $p_I = p_2$; a general expression for p_I consists in some weighted average of p_1 and p_2 and will therefore lead to an intermediate state between the ones on the figure (green and red ones) as can be seen for the particular case $p_I = \overline{p}$. This is an illustration on how the interfacial pressure – which is not present in the 5-equation model – impacts the physical solutions obtained by modifying the volume fraction jump condition that is enforced by the numerical scheme. This is because, unfortunately, the 5-equation model does not have a complete set of well-defined jump conditions; however note that the change in volume fraction observed is quite moderate when compared to the extreme pressure ratio used to generate it; thus indicating that the theoretical shortcomings of the model — the absence of a Rankine-Hugoniot condition for the volume fraction — might have only a limited impact for practical cases.

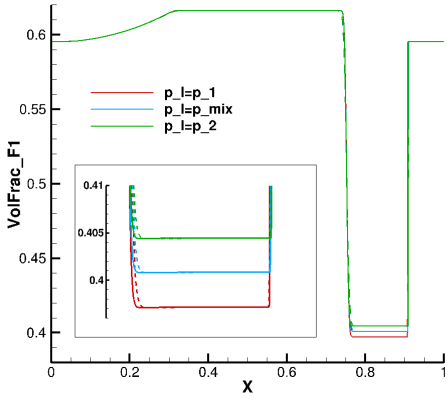

Figure 3: Epoxy volume fraction profiles obtained for the extreme epoxy-spinel shock case with different interfacial pressures ($p_I = p_1$, p_2 or $\overline{p}$ denoted p_{mix} in the legend) with zoom on the intermediate state. Two meshes are used : 4000 cells (dotted line) and 8000 cells (full line).

5.3 Shock-droplet interaction problem

The last test case we consider is a shock-droplet interaction case which has been studied experimentally in [28] and numerically using a 4-equation model in [25]. We focus on the early stage of the interaction. An axisymmetrical configuration is simulated, details on the initial conditions and the geometry are found in [25]. In pure regions, a residual volume fraction for the absent phase is set to 10^{-8}. We use the scheme with a MUSCL reconstruction of the primitive variables with a minmod limiter and a two-stage second order SSP Runge-Kutta method at CFL 0.3 in order to attain second order accuracy. Results for the instantaneous pressure relaxation scheme are shown in Figures 4 and 5. After the shock propagates through the droplet, a strong rarefaction wave is generated. Similarly to the double rarefaction wave problem (Section 5.1), negative liquid pressures after the hyperbolic step can cause erroneous energy exchanges and result in exceedingly high gas temperatures when the wrong interfacial pressure is used which will, in turn, affect the pressure profile (see Figure 4). Setting $p_I = p_1$ prevents negative interfacial pressures, but as with the implicit method [7], the scheme still leads to extreme gas temperatures, although less than with $p_I = \overline{p}$, and with a lesser impact on the pressure profile (see Figure 5).

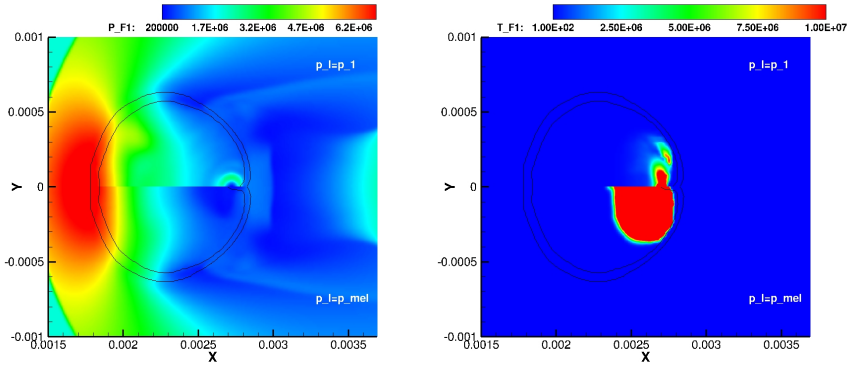

Figure 4: Pressure and gas temperature at $t = 3.5\,\mu s$ with interfacial pressure $p_I = p_1$ (top half) and $p_I = \overline{p}$ (bottom half). Black lines are volume fraction isolines $\alpha = 0.05$ and $\alpha = 0.95$.

In Figure 6, we have compared the results using the instantaneous pressure-temperature relaxation scheme with the results for the 4-equation model obtained using a second order HLLC scheme from [25]. The results for the early stage of the shock-droplet interaction are very similar, showing that with the instantaneous pressure-temperature relaxation we recover the solutions of the 4-equation model. Moreover, the method is more robust as the second order HLLC scheme was combined with a pressure threshold to ensure positivity while no such threshold was required during the computation with the relaxation scheme. Additionally, results in Fig. 6 show some numerical pressure oscillations along the droplet's interface for both HLLC schemes. This phenomena has been observed in previous works as it is well-known that finite volume schemes for the 4-equation model suffer from such oscillations through contact discontinuities with a non-uniform temperature [29]. On the contrary, as can be observed in Figs. 4 and 5, the 5-equation model does not suffer from this shortcoming and yields a smooth pressure profile. As a result, the 5-equation model is more suited for these type of high-velocity two-phase flow simulations provided as robust discretization is used; within our framework, this entails an appropriate choice for the interfacial pressure relaxation parameter (as well as a robust discretization of the homogeneous 6-equation model — see Sec. 3 — which will be discussed in a forthcoming paper).

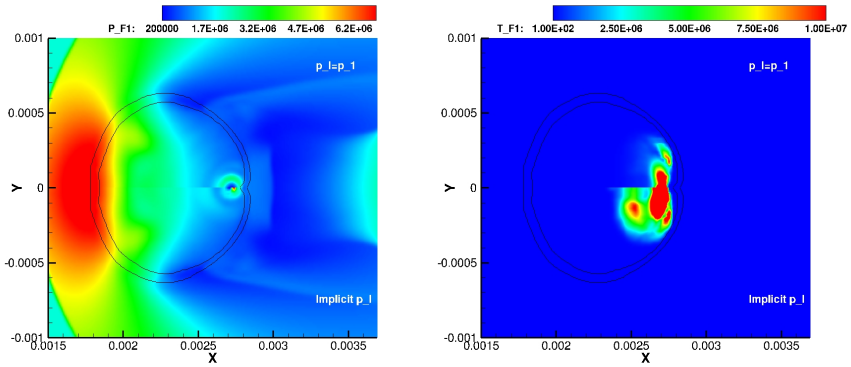

Figure 5: Pressure and gas temperature at $t = 3.5\,\mu s$ using the interfacial pressure $p_I = p_1$ (top half) and the implicit approximation method [7] (bottom half). Black lines are volume fraction isolines $\alpha = 0.05$ and $\alpha = 0.95$.

6 CONCLUSIONS

We have investigated the class of instantaneous relaxation schemes. Focus has been given on the role of interfacial pressure in instantaneous pressure relaxation schemes, which are widely

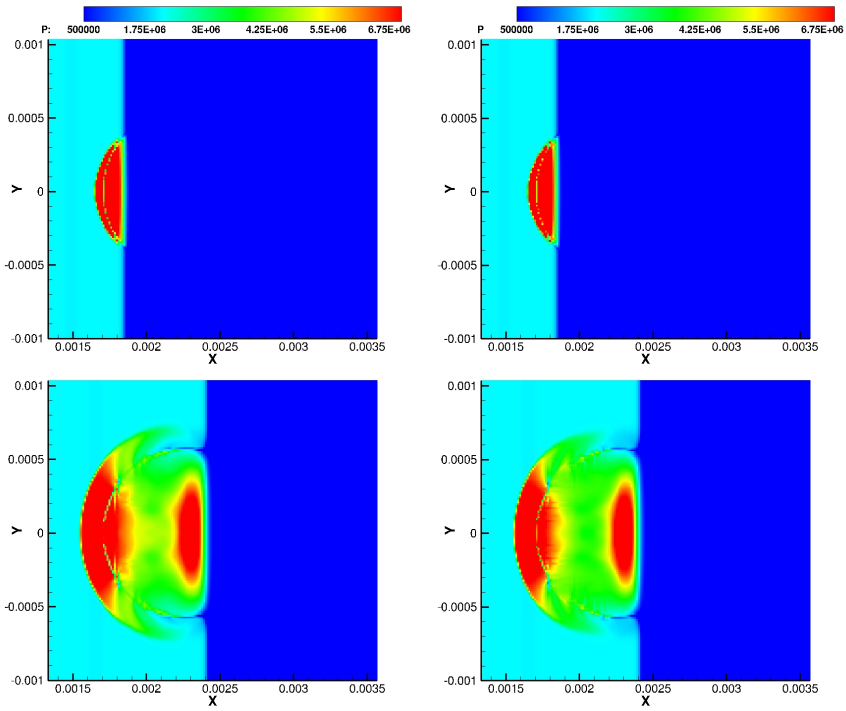

Figure 6: Pressure profiles obtained for the shock-droplet interaction case at times $t = 0.35\,\mu s$ (top) and $t = 0.74\,\mu s$ (bottom) by solving the 4-equation model with an instant pressure-temperature relaxation scheme (left) or by solving directly the 4-equation model (right) .

used to solve the 5-equation model [7, 8, 9]. As the interfacial pressure is not present in the 5-equation model, it is a free parameter of the numerical scheme that must be set by the user. As the model is non-conservative and does not have a complete set of jump conditions, weak solutions are not unique and different numerical schemes can converge to different solutions for strong shocks. Through a detailed discussion on the interfacial pressure, we have shown that this parameter may impact the convergence of the scheme to such solutions as it determines the thermodynamic path followed during the relaxation process as well as the resulting equilibrium state. Moreover, we have shown that the correct choice for this parameter can be paramount to ensure the robustness of the numerical scheme, whereas, for the pressure-temperature relaxation scheme, no interfacial pressure parameter is necessary as all thermodynamic paths lead to the same equilibrium state and the physical solutions of the 4-equation model are recovered. However, the pressure-temperature relaxation scheme suffers from other shortcomings, such as the pressure oscillations through contact discontinuities. Eventually, the two-temperature framework provided by the 5-equation model allows for the modelling of heat exchange at finite rate and phase change with thermal inertia while keeping a simple wave structure, unlike other models such as the 7-equation model [1] and we have proposed an efficient and accurate way of simulating this model, without additional cost compared to existing strategies, which offers an interesting strategy for high-speed flows.

This work was supported by the Agence Innovation Défense (AID) and the CIEDS project OPEN-NUM-DEF, whom we would like to acknowledge.

REFERENCES

[1] Baer, M. R. & Nunziato, J. W. *International Journal of Multiphase Flow* (1986). 12(6):861–889.

[2] Saurel, R. & Abgrall, R. *Journal of Computational Physics* (1999). 150(2):425–467.

[3] Kapila, A. K. et al. *Physics of Fluids* (2001). 13(10):3002–3024.

[4] Labois, M. Ph.D. thesis, Université de Provence - Aix-Marseille I (2008).

[5] Lund, H. *SIAM Journal on Applied Mathematics* (2012). 72(6):1713–1741.

[6] Murrone, A. & Guillard, H. *Journal of Computational Physics* (2005). 202(2):664–698.

[7] Saurel, R. et al. *Journal of Computational Physics* (2009). 228(5):1678–1712.

[8] Pelanti, M. & Shyue, K.-M. *Journal of Computational Physics* (2014). 259:331–357.

[9] Schmidmayer, K. et al. *International Journal for Numerical Methods in Fluids* (2023). 95(2):215–241.

[10] Schmidmayer, K. et al. *Journal of Computational Physics* (2017). 334:468–496.

[11] Wood, A. B. *A Textbook of Sound*. G. Bell and Sons Ltd., London (1930).

[12] Gallouët, T. et al. *Mathematical Models and Methods in Applied Sciences* (2004). 14(05):663–700.

[13] Coquel, F. et al. *Journal of Computational Physics* (2017). 330:401–435.

[14] Maso, G. et al. *Journal de Mathématiques Pures et Appliquées* (1995). 74:483–548.

[15] Le Floch, P. *Institute for Mathematics and Its Applications* (1989).

[16] Abgrall, R. & Karni, S. *Journal of Computational Physics* (2010). 229(8):2759–2763.

[17] Sainsaulieu, L. *SIAM Journal on Mathematical Analysis* (1996). 27(5):1286–1310.

[18] Wargnier, Q. et al. *SIAM Journal on Scientific Computing* (2020). 42(2):B492–B519.

[19] Liu, T.-P. *Communications in Mathematical Physics* (1987). 108(1):153–175.

[20] Natalini, R. Recent mathematical results on hyperbolic relaxation problems, analysis of systems of conservation laws, pitman research notes in mathematics series (1998).

[21] Bouchut, F. *Journal of Hyperbolic Differential Equations* (2004). 1(1):149–170.

[22] Gottlieb, S. et al. *Strong Stability Preserving Runge-Kutta and Multistep Time Discretizations*. World Scientific (2011).

[23] Jin, S. *Journal of Computational Physics* (1995). 122:51–67.

[24] Schmidmayer, K. et al. *Computer Physics Communications* (2020). 251:107093.

[25] Le Touze, C. & Rutard, N. In *8th European Congress on Computational Methods in Applied Sciences and Engineering*. CIMNE (2022) .

[26] Pelanti, M. *International Journal of Multiphase Flow* (2022). 153:104097.

[27] De Lorenzo, M. et al. *Applied Mathematics and Computation* (2018). 333:95–117.

[28] Hébert, D. et al. *SN Applied Sciences* (2020). 2(1):69.

[29] Abgrall, R. *Journal of Computational Physics* (1996). 125(1):150–160.